

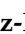




Article

Mechanochemical Synthesis and Structure of the Tetrahydrate and Mesoporous Anhydrous Metforminium(2+)-*N,N'*-1,4-Phenylenedioxalamic Acid (1:2) Salt: The Role of Hydrogen Bonding and $n \rightarrow \pi^*$ Charge Assisted Interactions

Sayuri Chong-Canto ¹, Efrén V. García-Báez ¹, Francisco J. Martínez-Martínez ²,
Angel A. Ramos-Organillo ² and Itzia I. Padilla-Martínez ^{1,*}

¹ Laboratorio de Química Supramolecular y Nanociencias, Instituto Politécnico Nacional-UPIBI, Av. Acueducto s/n Barrio la Laguna Ticomán, Ciudad de México C.P. 07340, Mexico; schongc0800@alumno.ipn.mx (S.C.-C.); egarciaba@ipn.mx (E.V.G.-B.)

² Facultad de Ciencias Químicas, Universidad de Colima, Km. 9 Carretera Colima-Coquimatlán, Coquimatlán C.P. 28400, Colima, Mexico; fmartin@ucol.mx (F.J.M.-M.); aaramos@ucol.mx (A.A.R.-O.)

* Correspondence: ipadillamar@ipn.mx; Tel.: +52-555-729-6000 (ext. 56324)

Received: 23 September 2020; Accepted: 18 October 2020; Published: 21 October 2020



Abstract: A new organic salt of metformin, an antidiabetic drug, and *N,N'*-(1,4-phenylene)dioxalamic acid, was mechanochemically synthesized, purified by crystallization from solution and characterized by single X-ray crystallography. The structure revealed a salt-type crystal hydrate composed of one dicationic metformin unit, two monoanionic units of the acid and four water molecules, namely $H_2Mf(HpOXA)_2 \cdot 4H_2O$. X-ray powder, IR, ^{13}C -CPMAS, thermal and BET adsorption–desorption analyses were performed to elucidate the structure of the molecular and supramolecular structure of the anhydrous microcrystalline mesoporous solid $H_2Mf(HpOXA)_2$. The results suggest that their structures, conformation and hydrogen bonding schemes are very similar. To the best of our knowledge, the selective formation of the monoanion $HpOXA^-$, as well as its structure in the solid, is herein reported for the first time. Regular $O(\delta^-) \cdots C(\delta)$, $O(\delta^-) \cdots N^+$ and bifacial $O(\delta^-) \cdots C(\delta) \cdots O(\delta^-)$ of $n \rightarrow \pi^*$ charge-assisted interactions are herein described in H_2MfA organic salts which could be responsible of the interactions of metformin in biologic systems. The results support the participation of $n \rightarrow \pi^*$ charge-assisted interactions independently, and not just as a short contact imposed by the geometric constraint due to the hydrogen bonding patterns.

Keywords: metformin cocrystal; mechanochemical synthesis; dicationic metformin; water channels; pi-interactions; mesoporous anhydrate

1. Introduction

Cocrystallization has become a growing discipline of interest in pharmaceutical sciences, since its application has been demonstrated to modify the physical-chemical properties of known drugs [1]. Metformin–HCl (HMfCl) is an oral anti-hyperglycemic drug, used worldwide for the treatment of non-insulin-dependent diabetes mellitus. It improves glucose tolerance, lowering plasma glucose levels and glycated hemoglobin, particularly in overweight and obese patients. Metformin is one of the most frequently used small molecules for preparing combined drugs such as Segluromet (metformin–ertugliflozin), Metaglip (metformin–glipizide) and Glucovance (metformin–glyburide). These are examples of the fourteen combinations approved by FDA [2], some of which have been characterized by monocrystal X-ray diffraction such as metformin–glimepiride [3] and

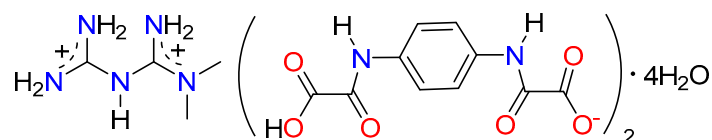
metformin–salicylic acid [4]. Due to its pharmaceutical importance, there is a great interest in metformin cocrystals, which has led to several patents related to the formation of organic salts, compiled elsewhere [5].

In addition, the structure and electronic structural details of metformin and its cocrystals have recently been summarized, in the context of biguanide compounds [6]. Metformin is a privileged small molecule; it possesses conformational flexibility and is capable of forming strong hydrogen bonding interactions, which will determine its structure and activity in biological processes. Metformin hydrochloride is known to crystallize into two conformational polymorphs, namely, A [7] and B [8]. The Me₂N–C–N–C backbone adopts the U conformation in the thermodynamic phase A (Me₂NCNC torsion angle value of 53.7°), whereas the form of an S backbone is observed in the metastable polymorph B (Me₂NCNC torsion angle value of 129.1°). The calculated minima are near 50° and 160°, respectively [9].

On the other hand, oxalamic or oxamic acids are the amide-carboxylic acid derivatives of the oxalic acid. They have been recognized because of their high potential in crystal engineering and molecular recognition due to their bifunctionality [10]. As far as *N,N'*-(1,4-phenylene)dioxalamic acid (H₂pOXA) and its 1,3-isomer (H₂mOXA) are concerned, they were first reported in the mid 1970s [11,12] as antiallergic agents as well as anti-inflammatory compounds [13]. More recently, both have attracted interest as coordinating ligands for metals [14,15]. Theoretical studies and experimental work [16] have demonstrated the high flexibility of the oxalic acid derivatives. Both oxalyl carbonyls are usually in *anti* disposition [17], but they less frequently adopt the *syn* disposition, induced by steric constraints [18,19] or by coordination with metals in the form of carboxylates [14].

Finally, mechanochemical synthesis consists of the application of mechanical energy to induce a chemical reaction, its use and applications have been recently reviewed [20]. Liquid-assisted grinding (LAG) makes use of some drops of solvent to provide greater molecular mobility in the course of the milling procedure. Even though the liquid does not play the role of solvent, it can be incorporated into the crystal network to form solvates or not.

Herein we report the LAG method for synthesizing the tetrahydrate, depicted in Scheme 1, and anhydrate of the antidiabetic drug metformin and *N,N'*-(1,4-phenylene)dioxalamic acid. Their molecular and supramolecular structures were analyzed in the context of the interactions of metformin in biologic systems.



Scheme 1. Molecular structure of the tetrahydrate of the antidiabetic drug metformin and *N,N'*-(1,4-phenylene)dioxalamic acid of formula H₂Mf(HpOXA)₂·4W.

2. Materials and Methods

2.1. Materials and Crystal Synthesis

Metformin hydrochloride (HMetCl) was isolated from commercial sources: 10 tablets of 500 mg were ground and suspended in 150 mL of ethyl alcohol (96%), the mixture was boiled under stirring for 10 min or until complete dissolution. The hot solution was filtered; crystals of HMfCl were obtained after cooling to room temperature to obtain 2.5 g of a white solid, which was analyzed by IR, NMR and single crystal X-ray diffraction, corresponding to the crystal structure reported by Hariharan [7]. The *N,N'*-(1,4-phenylene)dioxalamic acid double hydrate (H₂pOXA·2W, W = water) was obtained as reported elsewhere [14]. Single crystals of *N,N'*-(1,4-phenylene)dioxalamate of di-(metformin diammonium) tetrahydrate (H₂Mf(HpOXA)₂·4W) were harvested starting from 0.060 g (0.350 mmol) of HMfCl and 100 mg (0.347 mmol) H₂pOXA·2W which were grinded with a pestle in

a mortar with the aid of few drops of water for 33–45 min until a homogeneous paste was formed. This mass was suspended in 40 mL of water and boiled under stirring until a clear solution appeared. The solution was left to stand at room temperature and after two days, 0.113 g (0.16 mmol) of beige crystals suitable for X-ray analysis were obtained in 92% yield. Similar results were obtained using 1:2 stoichiometric amounts of HMfCl (0.030 mg) to H₂pOXA·2W (100 mg) to obtain 0.120 g (0.17 mmol) of H₂Mf(HpOXA)₂·4W in 98% yield. Microcrystalline powder of H₂Mf(HpOXA)₂ was obtained from single crystals of H₂Mf(HpOXA)₂·4W after drying at 100 °C for 2 h in an air oven.

2.2. Instrumental

IR spectra were recorded neat at 25 °C using a Perkin Elmer Spectrum GX series with FT system spectrophotometer using the ATR device. ¹³C-CPMAS spectra were recorded on a Bruker Avance DPX-400 (101 MHz). The following conditions were applied: spectral width 30.242 kHz, acquisition time 33.8 ms, contact time 2000 ms, rotation rate 8 kHz, relaxation delay 5 s, and up to 256 scans for each spectrum were collected. Room temperature X-ray powder diffraction data were collected on a PAN Analytical X'Pert PRO diffractometer with Cu Kα1 radiation (λ = 1.5405 Å, 45 kV, 40 mA) or on a D8 Focus Bruker AXS instrument using Cu Kα1 radiation (λ = 1.542 Å, 35 kV, 25 mA). Texture analysis of H₂Mf(HpOXA)₂ was performed in an ASAP-2050 Xtended Pressure Sorption Analyzer of Micromeritics. Prior to measurement, vacuum sample activation was performed for 10 min to 150 °C, the measuring temperature was 75.15 K and it was maintained through a liquid nitrogen dewar. The gas used for the analysis was N₂ (gas). For measurements, 40.8 mg of the activated mass sample were taken. DSC and TG measurements were performed in a Q2000 equipment and a Thermobalance Q5000 IR, respectively, of TA instruments. In both cases, approximately 3.0–5.0 mg of sample was used and a gradient of 5.00 °C/min from room temperature to 350 °C under air flux of 25 mL/min in an open (TG) or pin-holed panels (DSC).

2.3. X-ray Structure Determination

General crystallographic data for H₂Mf(HpOXA)₂·4W has been deposited in the Cambridge Crystallographic Data Centre (CCDC) as supplementary publication number 1874280. Single crystal X-ray diffraction data were collected on an Agilent SuperNova (dual source) diffractometer using graphite-monochromatic Mo (λ = 0.71073 Å) Kα radiation; data collection, cell refinement and data reduction were accomplished using CrysAlisPro software [21]. The structure was solved by direct methods using the SHELXS program [22] of the WINGX package [23]. The final refinement was performed by full-matrix least-squares methods using the SHELXTL-2018/3 program [24]. The H atoms on C, N, and O were geometrically positioned and treated as riding atoms with: C–H 0.93–0.98 Å, Uiso(H) = 1.2 eq(C) for aromatic carbon atoms or 1.5 eq(C) for methyl carbon atoms; O–H = 0.82 Å, Uiso(H) = 1.5 eq(O); N–H = 0.86 Å, Uiso(H) = 1.2 eq(N). Platon [25] and Mercury [26] were used to prepare the material for publication.

Crystal Data for 2(C₁₀H₇N₂O₆)·(C₄H₁₃N₅)·4(H₂O), (H₂Mf(HpOXA)₂·4W), M = 705.61 g/mol: triclinic, space group *P*-1, a = 8.1357 (11), b = 13.8594 (18), c = 14.4846 (13) Å, α = 109.963 (10)°, β = 92.453 (9)°, γ = 95.863 (11)°, V = 1521.8 Å³, Z = 2, T = 293 K, μ(MoKα) = 0.71073 Å, D_{calc} = 1.540 g/cm³, 10,558 reflections measured (3.0° ≤ 2θ ≤ 52.57°), 5941 unique (R_{int} = 0.027, R_{sigma} = 0.034), which were used in all calculations. The final R1 was 0.047 (I > 2σ (I)) and wR2 was 0.138 (all data).

3. Results and Discussion

3.1. Synthesis

Microcrystalline solid phase of *N,N'*-(1,4-phenylene)dioxalamate of di-(metformin diammonium) tetrahydrate (H₂Mf(HpOXA)₂·4W) was synthesized using a water-assisted grinding procedure. Two stoichiometric proportions were used of HMfCl/H₂pOXA: 1:1 and 1:2. In both cases, the reaction was monitored to completion by comparing the XRPD patterns of the mixtures to the pristine HMfCl,

Figure 1. Single crystals of $\text{H}_2\text{Mf}(\text{HpOXA})_2 \cdot 4\text{W}$ organic salt were obtained by recrystallization from hot water of either of the two grinded mixtures. The reaction is quantitative based on the stoichiometry of the following reaction:

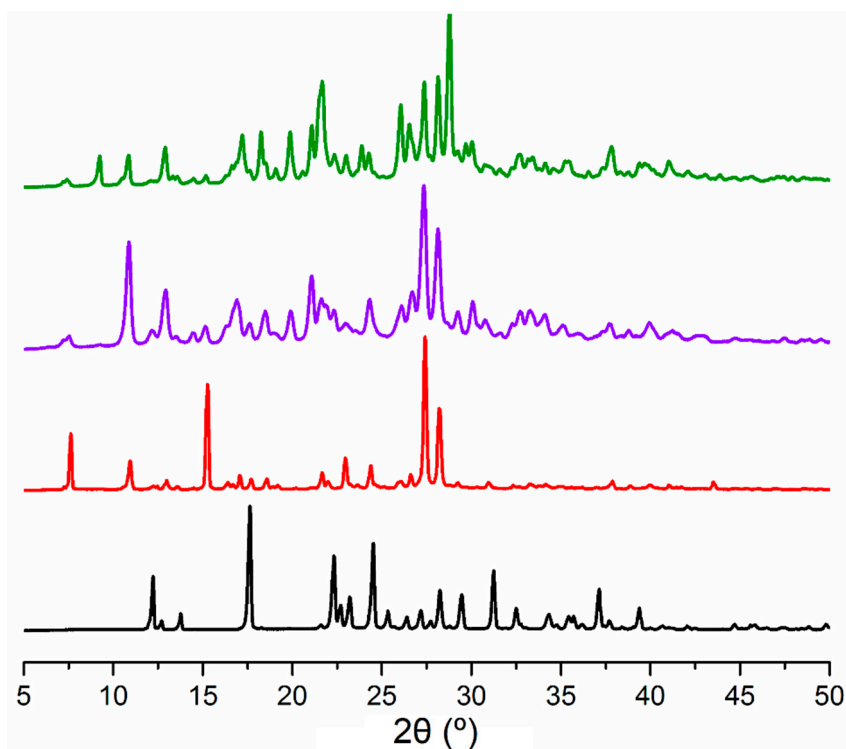
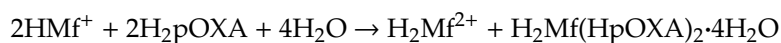


Figure 1. XRPD patterns of (a) pristine HMfCl, (b) $\text{H}_2\text{Mf}(\text{HpOXA})_2 \cdot 4\text{W}$ organic salt (experimental), (c) mechanochemical synthesis in 1:1 proportion of HMfCl/ H_2pOXA , and (d) mechanochemical synthesis in 1:2 proportion of HMfCl/ H_2pOXA .

The proton of one carboxylic acid group of H_2pOXA is transferred to the remaining basic nitrogen site of HMfCl molecule to form the H_2Mf^{2+} dication and the monoanion of N,N' -(1,4-phenylene)dioxalamic acid (HpOXA^-), which crystallize from the aqueous solution as $\text{H}_2\text{Mf}(\text{HpOXA})_2 \cdot 4\text{W}$ organic salt. Therefore, even when it can be obtained by a milling procedure in the solid state, the crystallization step from aqueous solution is required in order to eliminate the remaining H_2MfCl_2 byproduct.

Microcrystalline powder of $\text{H}_2\text{Mf}(\text{HpOXA})_2$ was obtained from single crystals of $\text{H}_2\text{Mf}(\text{HpOXA})_2 \cdot 4\text{W}$ after drying at 100°C for 2 h in an air oven.

3.2. The Molecular and Supramolecular Structure of $\text{H}_2\text{Mf}(\text{HpOXA})_2 \cdot 4\text{W}$

The salt $\text{H}_2\text{Mf}(\text{HpOXA})_2 \cdot 4\text{W}$ crystallizes in the triclinic system, space group $P-1$ with one, two and four independent units of H_2Mf^{2+} , HpOXA^- and H_2O in the asymmetric unit, respectively, and whose molecular structure is depicted in Figure 2.

The oxalyl fragments COCO are almost planar, with a mean O–C–C–O angle of $179.3(6)^\circ$. However, small differences can be noted between the oxalamic acid NCOCO_2H and oxalamate fragments, NCOCO_2^- . The NCOCO_2H endings are located slightly out of plane of the corresponding benzene ring, the maximum deviations from planarity are presented by N7C8O8C9O9O10H10 and N27C28O28C29O29O30H30 fragments with torsion angles of $16.08(5)^\circ$ and $9.83(6)^\circ$ from the C1–C6 and C21–C26 rings, respectively. Instead, the oxalamate counterparts NCOCO_2^- are almost coplanar to the corresponding benzene ring: $3.50(6)^\circ$ for N17C18O18C19O19O20 and $5.02(6)^\circ$ for

N37C38O38C239O39O40. It is worth noting that NCOCO₂H and NCOCO₂[−] arms are in *syn* disposition between each other (*sp-sp* conformation). It is worth mention that this conformation has not been observed among organic cocrystals of H₂pOXA but is commonly attained by coordination to metals [27]. The calculated conformational landscape of 1,4-phenylen dioxalyls predicts a very small difference in energy between planar *ap-sp* and *sp-sp* conformers of 0.26–0.28 kcal mol^{−1}, in favor of the former, and an interconversion energy of only 4.80 kcal mol^{−1} [16]. Then, the *sp-sp* conformation exhibited by the HpOXA[−] moiety is explained because of the stabilization given by hydrogen bonding with metformin that provides the energy to overcome the rotational barrier.

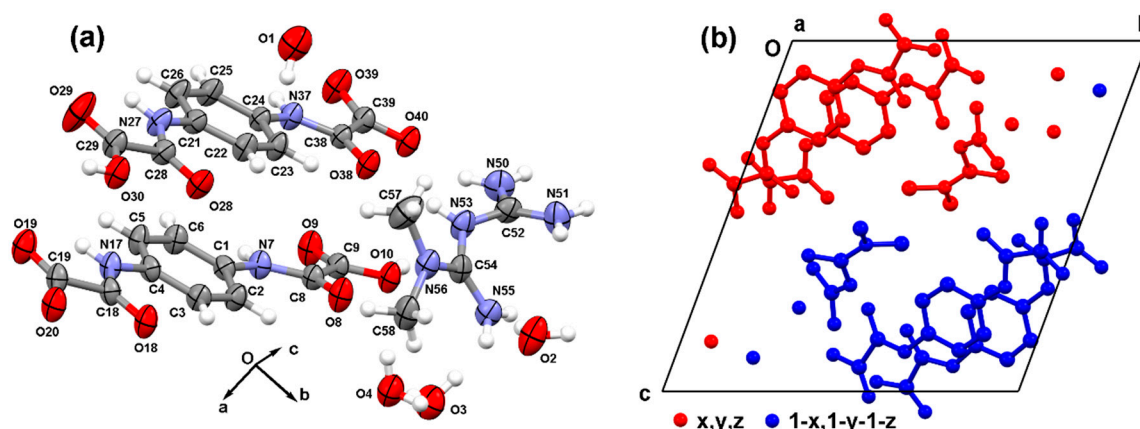


Figure 2. (a) Molecular structure of the organic salt H₂Mf(HpOXA)₂·4W showing the atom labelling scheme, displacement ellipsoids are drawn at the 50% probability level. (b) Unit cell picture in the *bc* plane showing two units of H₂Mf(HpOXA)₂·4W (*Z* = 2) and symmetry codes, hydrogen atoms are omitted.

The C(*sp*²)–N(*sp*²) bond lengths of the metformin dication moiety range from 1.302(3) to 1.378(3) Å. In fact, the bond lengths of C52 and C54 with the terminal nitrogen atoms are shorter, whereas the corresponding bond lengths with the bridge N53 atom are longer, than those bonds observed in monocationic metformin (1.333–1.341 Å) [28]. These last bond lengths have values close to those observed in five-membered heterocycles involving pyrrolic nitrogen (≈1.37 Å) [29]. In agreement, the proposed delocalized structure is depicted in Figure 3. Selected bond lengths and torsion angles are listed in Table 1. In H₂Mf(HpOXA)₂·4W, the two planar guanidinium halves N53C54N55N56 and N53C52N51N50, are twisted by 55.67(9)° and the NMe₂ group is located opposite to the C(NH₂)₂ group (N56C54N53C52 torsion angle value of 148.8(2)°).

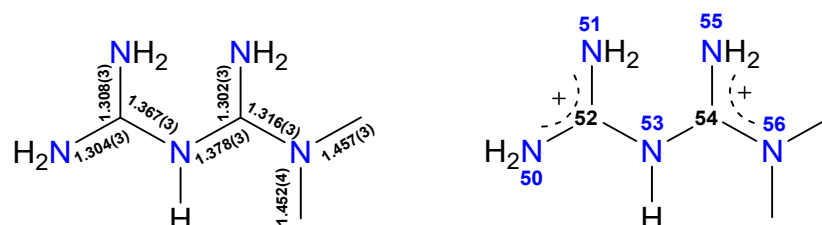


Figure 3. Bond lengths in Å (left) and delocalized structure of the dicationic metformin H₂Mf²⁺ (right) showing the atom numbering scheme.

Table 1. Selected bond lengths and torsion angles of the organic salt $H_2Mf(HpOXA)_2 \cdot 4W$.

HpOXA [−] Moiety			
Atoms	Bond Lengths/Å	Atoms	Bond Lengths/Å
C8–C9	1.534(3)	C18–C19	1.556(3)
C28–C29	1.542(3)	C38–C39	1.550(3)
Torsion Angles/°		Torsion Angles/°	
C2–C1–N7–C8	−16.7(4)	C3–C4–N17–C18	−2.7(4)
O8–C8–N7–C1	1.5(4)	O8–C8–C9–O9	−179.7(2)
O18–C18–N17–C4	1.1(4)	O18–C18–C19–O19	177.0(2)
C22–C21–N27–C28	−11.1(4)	C23–C24–C25–C26	−1.1(3)
O28–C28–N27–C21	2.4(4)	O28–C28–C29–O29	−178.8(2)
O28–C28–N27–C21	2.4(4)	O28–C28–C29–O29	−178.8(2)
O38–C38–N37–C24	4.8(4)	O38–C38–C39–O39	−171.6(2)
H ₂ Mf ²⁺ Moiety			
Atoms	Bond Lengths/Å	Atoms	Bond Lengths/Å
N50–C52	1.304(3)	N51–C52	1.308(3)
N53–C52	1.367(3)	N53–C54	1.378(3)
N55–C54	1.302(3)	N56–C54	1.316(3)
N56–C58	1.457(3)	N56–C57	1.452(4)
Torsion Angle/°			
N56–C54–N53–C52	148.8(2)		

In the salt $H_2Mf(HpOXA)_2 \cdot 4W$, the metforminium moiety adopts the S backbone conformation, which has been reported as the most stable, owing to the decreased van der Waals repulsion, greater π -electron delocalization and intramolecular hydrogen bonding [9]. The structure of metformin in the $H_2Mf(HpOXA)_2 \cdot 4W$ is very similar to that observed in the monohydrates of dicationic 1:1 salts of formula $H_2MfA \cdot H_2O$ (A = oxalate, sulfate) [30], supporting that the anions slightly influence the structure of *N,N*-dimethylbiguanidinium moiety.

The H_2Mf^{2+} and both $HpOXA^-$ moieties are attached to each other through $N53-H53 \cdots O38$ and $N50-H50B \cdots O40$, which lead to $R^2_2(9)$ hydrogen bonding ring motif and $N51-H51B \cdots O18$ hydrogen bonding interactions. Four water molecules, forming amide \cdots water interactions of bifurcated type in $R^1_2(6)$ ring motif ($Nn-Hn \cdots Om \cdots Hp-Cp$; $n = 7, 17$; $m = 3, 1$; $p = 6, 5$), water \cdots carboxylate ($O2-H2B \cdots O19^-$) and water \cdots water ($O3-H3A \cdots O4$) hydrogen bonding interactions, complete this basic repetition unit, Figure 4a. A duplex is formed by an inversion center of symmetry linked by $N55-H55B \cdots O28$ hydrogen bonding, $n \rightarrow \pi^*$ charge assisted interactions between $O8 \cdots C54 \cdots O18$, $O8 \cdots N56$, Figure 4b and several $CO \cdots CO$ interactions. The geometric parameters associated with these interactions are listed in Table 2. It is worth mention that the $C \cdots A$ distances (A = O, N) are smaller than the sum of the van der Waals radii of the involving atoms ($r_{VDW} = 1.70$ (C), 1.55 (N), 1.50 (O) Å) [31], and the $C=O \cdots C=O$ and $C=O \cdots N$ angles are in agreement with sheared parallel and perpendicular motifs, respectively [32]. Double strands are generated through acid \cdots carboxylate ($On-Hn \cdots Om^-$; $n = 10, 30$; $m = 40, 20$), Figure 5a, and $N50-H50B \cdots O40$ hydrogen bonding, Figure 5b. Meanwhile, the second dimension is developed by water \cdots $HpOXA^-$ interactions ($On-Hn \cdots Om^-$; $n = 2, 4$; $m = 39, 29$), $N37-H37 \cdots O1$ and $N55-H55A \cdots O2$, to form double layers within the (1 1 $\bar{1}$) plane, Figure 5b. A view along the direction perpendicular to this plane let us note two well-defined regions of metformin and water, Figure 5c. The distance between two $HpOXA^-$ chains is longer in the metformin region than in the water region, in order to accommodate the NMe_2 group, with mean values of 7.4(3) Å and 4.1(3) Å, respectively (distances measured between benzene ring edges). Finally, water molecules link the bilayers to develop the third dimension along the [0 1 1] direction ($N27-H27 \cdots O2$, $N50-H50A \cdots O4$, $N51-H51A \cdots O4$, $O1-H1A \cdots O3$, $O1-H1B \cdots O19$,

O3–H3B...O39, O4–H4A...O8 and O4–H4A...O10). The water molecules labelled as H₂O1 (W1), H₂O3 (W3) and H₂O4 (W4) form an open cluster, but together with H₂O2 (W2) are located in isolated pockets of the crystal lattice. The geometric parameters associated with intermolecular hydrogen bonding are listed in Table 3.

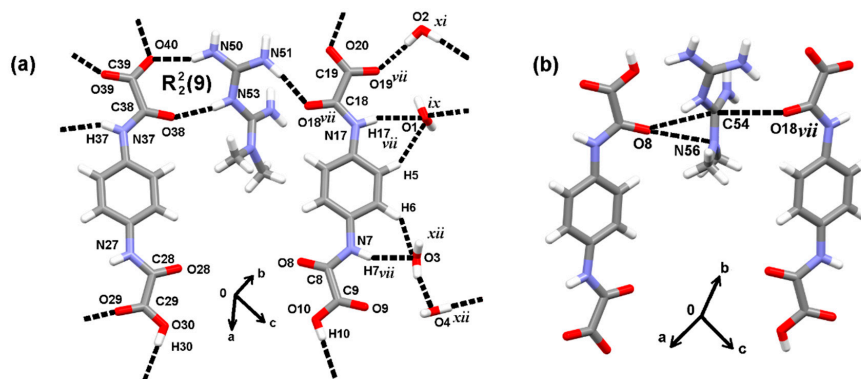


Figure 4. (a) Basic repetition unit of the organic salt H₂Mf(HpOXA)₂·4W and atom labelling scheme. (b) n→π* charge-assisted interactions between O8...C54...O18 and O8...N56 that contribute to form the duplex by an inversion center of symmetry. See Tables 2 and 3 for symmetry codes.

Table 2. Geometric parameters of CO...A interactions (A = CO, N) in H₂Mf(HpOXA)₂·4W.

C–O...A	C–O/Å	O...A/Å	C–O...A/°
C38–O38...C9	1.219(2)	3.083(3)	89.0(2)
C38–O38...C8	1.219(2)	3.075(3)	102.1(2)
C29–O30...C19	1.264(3)	3.198(3)	97.4(2)
C8–O8...C54	1.222(2)	3.142(3)	133.4(2)
C8–O8...N56	1.222(2)	3.003(3)	143.6(2)
C18–O18 vii...C54	1.222(3)	3.109(3)	131.8(2)

(vii) $-x + 1, -y + 1, -z + 1$.

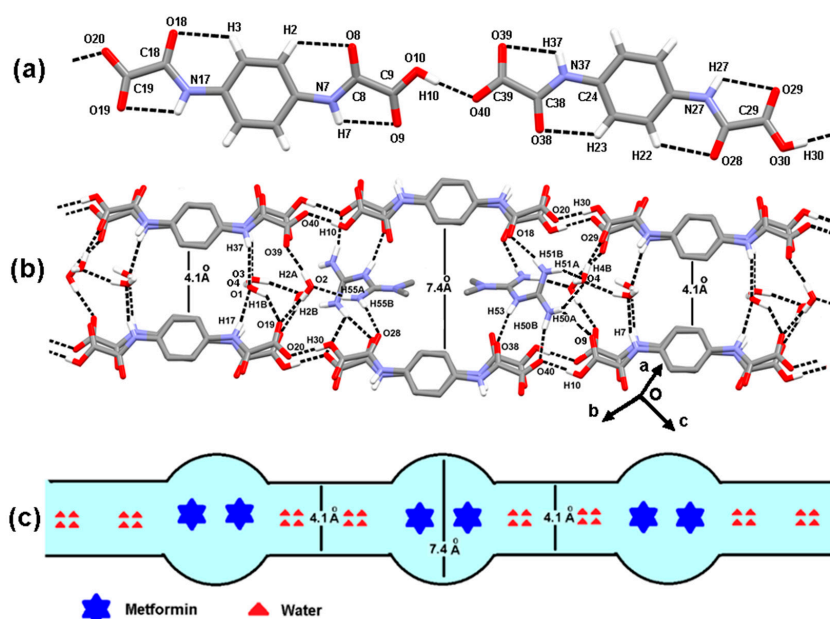


Figure 5. (a) Acid...carboxylate hydrogen bonding between the two units of HpOXA⁻. (b) Double strands of H₂Mf(HpOXA)₂·4W propagating along the (1 1 -1) plane. (c) Pictorial representation of H₂Mf(HpOXA)₂·4W where metformin diammonium and water pockets are highlighted.

Table 3. Intermolecular hydrogen bonding geometric parameters of H₂Mf(HpOXA)₂·4W.

D–H...A	D–H/Å	H...A/Å	D...A/Å	D–H...A/°
C5–H5...O1 ⁱ	0.93	2.62	3.438 (3)	147
C6–H6...O3 ⁱⁱ	0.93	2.48	3.217 (3)	136
N7–H7...O3 ⁱⁱ	0.86	2.17	2.991 (2)	159
N17–H17...O1 ⁱ	0.86	2.37	3.208 (3)	166
N27–H27...O2 ⁱⁱⁱ	0.86	2.58	3.154 (3)	125
N37–H37...O1 ^{iv}	0.86	2.49	3.185 (3)	139
N50–H50B...O40	0.86	2.02	2.820 (3)	154
N50–H50A...O4 ^v	0.86	2.27	2.999 (3)	143
N50–H50A...O9 ^{vi}	0.86	2.37	2.982 (2)	129
N51–H51A...O4 ^v	0.86	2.20	2.947 (3)	145
N51–H51B...O18 ^{vii}	0.86	2.10	2.918 (2)	159
N53–H53...O38	0.86	2.00	2.843 (2)	168
N55–H55A...O2	0.86	1.92	2.730 (2)	157
N55–H55B...O28 ^{vii}	0.86	2.05	2.832 (2)	151
O1–H1A...O3 ^{vii}	0.85	2.15	2.985 (3)	169
O1–H1B...O19 ⁱ	0.85	2.33	2.998 (3)	136
O2–H2A...O39 ^{vi}	0.85	1.89	2.742 (2)	177
O2–H2B...O19 ^{viii}	0.85	1.93	2.760 (2)	166
O3–H3A...O4	0.85	1.93	2.760 (3)	167
O3–H3B...O39 ^{vi}	0.85	2.16	2.982 (3)	161
O4–H4A...O8	0.85	2.00	2.773 (3)	151
O4–H4A...O10	0.85	2.64	3.145 (2)	120
O4–H4B...O29 ^{ix}	0.85	1.80	2.611 (3)	160
O10–H10...O40 ^{vi}	0.82	1.72	2.5362 (19)	176
O30–H30...O20 ^x	0.82	1.66	2.477 (2)	177

Symmetry codes: (i) $-x + 1, -y, -z + 1$; (ii) $-x + 1, -y + 1, -z$; (iii) $x, y - 1, z$; (iv) $x, y, z - 1$; (v) $x - 1, y, z$; (vi) $-x, -y + 1, -z$; (vii) $-x + 1, -y + 1, -z + 1$; (viii) $x - 1, y + 1, z$; (ix) $x, y + 1, z$; (x) $-x + 2, -y, -z + 1$.

3.3. The Synthesis, Molecular and Supramolecular Structures of H₂Mf(HpOXA)₂ Anhydrate

Several techniques, such as IR and ¹³C-CPMAS spectroscopies, X-ray powder diffraction (XRPD), and thermal and BET-adsorption analyses, were performed in order to elucidate the molecular and supramolecular structure of the microcrystalline anhydrate of formula H₂Mf(HpOXA)₂.

The salt H₂Mf(HpOXA)₂·4W exhibits a sequence of two weight losses at peak temperatures of 65 °C and 113 °C as endothermic processes, that correspond to the release of one (exp. 2.6%, calcd. 2.7%) and three water molecules (exp. 7.8%, calcd. 8.1%) per formula unit, respectively; Figure 6. The remaining solid is stable between 150 and 200 °C and decomposes at a peak temperature of 212–214 °C, releasing the equivalent to 53% of the initial mass; Figure 6. Thus, a new microcrystalline phase of composition H₂Mf(HpOXA)₂ was obtained after air drying at 100 °C, this anhydrate rehydrates into the original tetrahydrate under 100% RH at 40 °C. The XRPD patterns that confirm the crystallinity and change in the solid phases are shown in Figure 7.

A summary of the IR wavenumbers of H₂Mf(HpOXA)₂ tetrahydrate and anhydrate compared to HMfCl are listed in Table 4, and the corresponding IR spectra are shown in Figure 8. The νC=O stretching bands of the carboxylic acid and amide groups as well as the νC=N wavenumbers are red shifted in comparison to the starting H₂pOXA·2W and HMfCl as a result of hydrogen bonding interactions. As far as the carboxylate group is concerned, it appears at 1524 cm⁻¹ in both H₂Mf(HpOXA)₂·tetrahydrate and anhydrate, more red shifted than the reported value of 1540 cm⁻¹ for the K₂pOXA salt [14], which is in agreement with a highly delocalized structure. It is worth noting that dehydration considerably clears the spectral window between 3500 and 3000 cm⁻¹ allowing the observation of the νN–H bands of the metformin moiety, which are observed in pairs in the IR spectrum of compound H₂Mf(HpOXA)₂, but the νN–H bands corresponding to the amide could not be assigned with certainty.

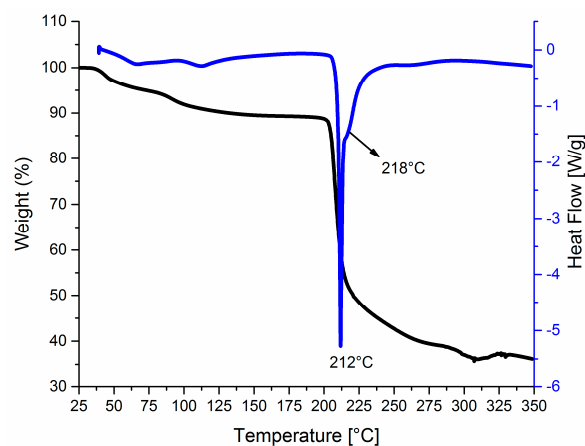


Figure 6. Tg, in black, and DSC, in blue, of $H_2Mf(HpOXA)_2 \cdot 4W$.

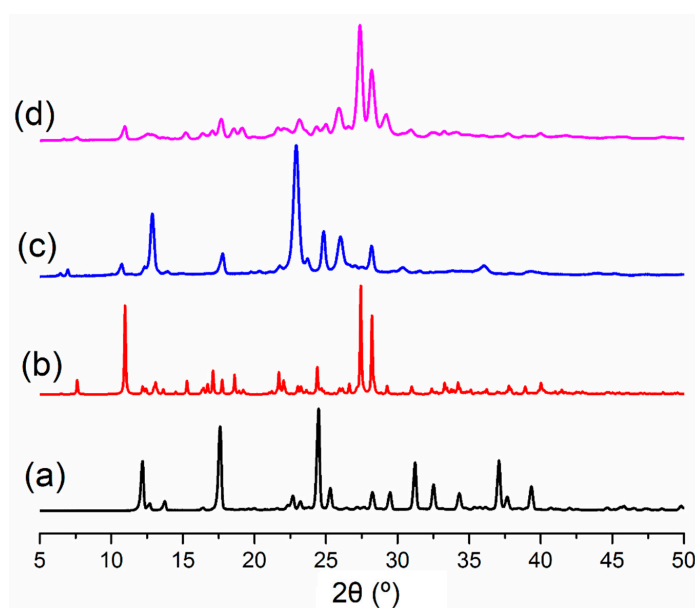


Figure 7. XRPD patterns of (a) pristine HMfCl, (b) $H_2Mf(HpOXA)_2 \cdot 4W$ organic salt simulated from single crystal X-ray data, (c) $H_2Mf(HpOXA)_2$ microcrystalline powder and (d) after rehydration from $H_2Mf(HpOXA)_2$.

Table 4. Stretching IR absorptions of solid powders of compounds H_2pOXA , HMfCl, $H_2Mf(HpOXA)_2 \cdot 4W$ and $H_2Mf(HpOXA)_2$.

Compounds	Bond Wavenumber (cm^{-1})			
	O–H	N–H	C=O	C=N
$H_2pOXA \cdot 2W$ ^a	3488 (br), 3349 (br)	3335 (m), 3307 (m)	1733 (m), 1714 (m), 1681 (s), 1657 (s)	
HMfCl		3390 (sh), 3379 (m) 3298 (br), 3155 (m) 3095 (sh)		1624 (m), 1584 (sh), 1585 (s), 1550 (s)
$H_2Mf(HpOXA)_2 \cdot 4W$	3442 (br), 3102 (br)	3432 (br), 3358 (br), 3334 (w), 3317 (w) 3445 (w), 3414 (w)	1686 (vs), 1524 (vs, COO ⁻)	1672 (sh)
$H_2Mf(HpOXA)_2$	3045 (br, m), 3180 (vw)	3372 (w), 3348 (w) 3329 (sh), 3309 (w)	1707 (sh), 1681 (s), 1524 (vs, COO ⁻)	1650 (sh), 1524 (sh) 1500 (vs)

^a From reference [14].

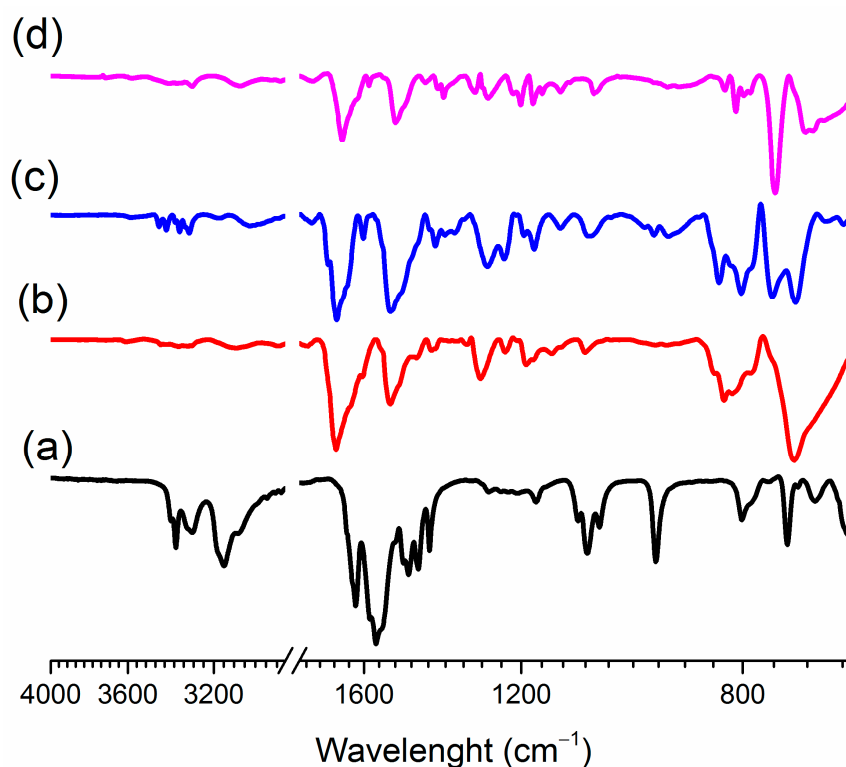
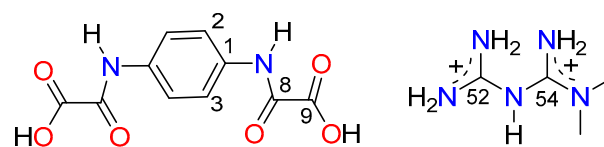


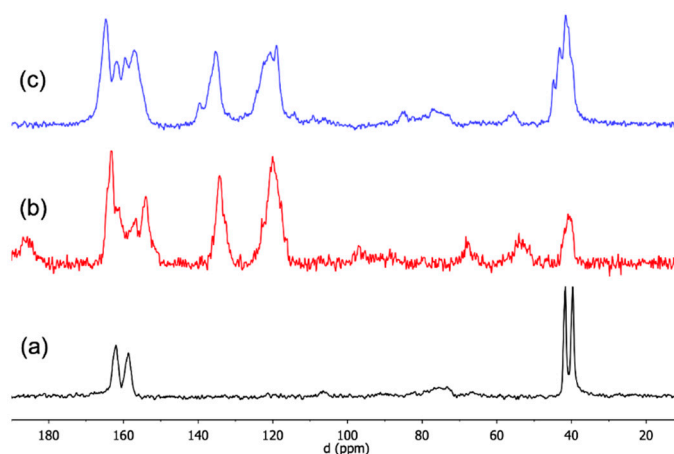
Figure 8. IR spectra of (a) metformin hydrochloride (HMfCl), (b) $\text{H}_2\text{Mf}(\text{HpOXA})_2 \cdot 4\text{W}$, (c) $\text{H}_2\text{Mf}(\text{HpOXA})_2$ and (d) $\text{H}_2\text{Mf}(\text{HpOXA})_2 \cdot 4\text{W}$ after rehydration from $\text{H}_2\text{Mf}(\text{HpOXA})_2$.

On the other hand, the ^{13}C -CPMAS provides useful information regarding the molecular and supramolecular structure. The chemical shift data are listed in Table 5 and spectra are depicted in Figure 9. The chemical shift of the amide carbonyl (C8O) is sensitive to the change in the hydrogen bonding environment, it is spread over a 155–159 ppm range, in response to the hydrogen bonding scheme in the crystal lattice of $\text{H}_2\text{Mf}(\text{HpOXA})_2 \cdot 4\text{W}$. Meanwhile, both COOH and COO[−] groups appear as one signal slightly shifted by ~2 ppm to high frequencies compared to the starting $\text{H}_2\text{pOXA} \cdot 2\text{W}$. This result is similar to that found in other carbonyls because of hydrogen bonding [33]. The *sp-sp* disposition between both oxalyl groups, in relation to the phenyl plane, and the presence of two independent molecules of HpOXA[−] in the asymmetric unit, as well as hydrogen bonding, have the effect of spreading the CH signals of the benzene ring in the 121–118 ppm range. The loss of water molecules opens the spectral window from 123 to 117 ppm and shifts the amide carbonyl to low frequencies by ~2 ppm. The chemical shifts of the dicationic metformin moieties, in both tetrahydrate and anhydrate organic salts of $(\text{H}_2\text{Mf})(\text{HpOXA})_2$, are the same as those observed in the monocationic HMfCl, except that the value of the carbon atom in the C(NH₂)NMe₂ fragment is shifted by ~2 ppm towards high frequencies, which is in agreement with increased delocalization and positive charge (*vide supra*). The analysis of the vibrational spectra and ^{13}C -CPMAS NMR data of $\text{H}_2\text{Mf}(\text{HpOXA})_2 \cdot 4\text{W}$ and its anhydrate suggest that their structures, conformation and hydrogen bonding schemes of both organic salts are very similar between them, with the exception of those regions formerly occupied by water molecules. Rehydration experiments performed on the $\text{H}_2\text{Mf}(\text{HpOXA})_2$ anhydrate, which reversibly rehydrates to the tetrahydrate, support these findings.

Table 5. CPMAS and isotropic ^{13}C chemical shifts of H_2pOXA , HMfCl , $\text{H}_2\text{Mf}(\text{HpOXA})_2\cdot 4\text{W}$ and $\text{H}_2\text{Mf}(\text{HpOXA})_2$.


Compounds	C1	C2	C3	C8O	C9O	C52	C54	CH ₃
H_2pOXA ^a	134.6	121.0	121.0	157.1	162.6			
HMfCl ^a						158.9	159.6	37.9
HMfCl crystals						159	162	42, 40
$(\text{H}_2\text{Mf})(\text{HpOXA})_2\cdot 4\text{W}$	136 ^b 134, 132	120 118 ^c	121 ^b 120 ^c	159 ^b 155 ^b	164 ^d	159	160	42, 40
$(\text{H}_2\text{Mf})(\text{HpOXA})_2$	136 134 ^c	119, 118 ^b 117	123 120 ^c	157 154	164 163	159	160	42, 41

^a in DMSO-d_6 solution; ^b 2C; ^c 3C; ^d 4C.

**Figure 9.** ^{13}C -CPMAS (a) pristine HMfCl , (b) $\text{H}_2\text{Mf}(\text{HpOXA})_2\cdot 4\text{W}$ organic salt, and (c) $\text{H}_2\text{Mf}(\text{HpOXA})_2$ microcrystalline powder.

Rehydration experiments performed on the $\text{H}_2\text{Mf}(\text{HpOXA})_2\cdot \text{anhydrate}$, which reversibly rehydrates to the tetrahydrate $\text{H}_2\text{Mf}(\text{HpOXA})_2\cdot 4\text{W}$, support the above findings. Furthermore, dehydration of $\text{H}_2\text{Mf}(\text{HpOXA})_2\cdot 4\text{W}$ can be associated with the role of water molecules in its crystal structure. As mentioned before, it occurred in two steps: one water molecule is lost at 65°C followed by three more at 113°C before decomposition. Judging by the number of hydrogen bonds and their strength, the water molecule labelled as W2 can be assigned to the first loss; it forms strong hydrogen bonds with amide and metformin NH in the crystal, as well as acting as a bridge between two HpOXA^- moieties of parallel chains; see Figure 5. Meanwhile, the water molecules labelled as W1, W3 and W4 form similar hydrogen bonds in number and nature as W2, but they are clustered together (vide supra), therefore leaving the crystal lattice at higher temperature. The removal of all water molecules from the isolated pockets of $\text{H}_2\text{Mf}(\text{HpOXA})_2\cdot 4\text{W}$ results in a stable framework given by the ionic interactions of the H_2Mf^{2+} dication and two units of the HpOXA^- monoanion. This framework is stable and capable of rearranging in the presence of moisture, restoring the microcrystalline lattice of the original tetrahydrate. A similar behavior was observed in sitafloxacin hydrate [34]. The formation of microporous channels in the structure of $\text{H}_2\text{Mf}(\text{HpOXA})_2$ was disregarded with a BET adsorption experiment, Figure 10a, which resulted in type III isotherm, characteristic of mesoporous solids [35], with pore size of $\sim 16\text{ nm}$, pore volume of $29\text{ mm}^3\text{ g}^{-1}$ and surface area of $7.7\text{ m}^2\text{ g}^{-1}$. The formation of large pores is in agreement with the ordered water detaching from the crystal structure, making available space along which water

can diffuse during rehydration. In addition, the observed hysteresis loop, of type H3, indicates the presence of macropores and plate-like particles. Thus, the main role of the water in the crystal lattice of $H_2Mf(HpOXA)_2 \cdot 4W$ is proposed not only to compensate the excess of donors given by the metformin moiety, but also to provide the hydrogen bonding interactions to build the third dimension in the crystal lattice. The examination of the $H_2Mf(HpOXA)_2 \cdot 4W$ crystal lattice allows us to propose that most of the original hydrogen bonding interactions as well as $n \rightarrow \pi^*$ charge-assisted interactions in the (0 1 1) plane are preserved after dehydration. Meanwhile, the (1 1 -1) plane is weakened after water loss, to form the $H_2Mf(HpOXA)_2$ mesoporous solid phase, Figure 10b.

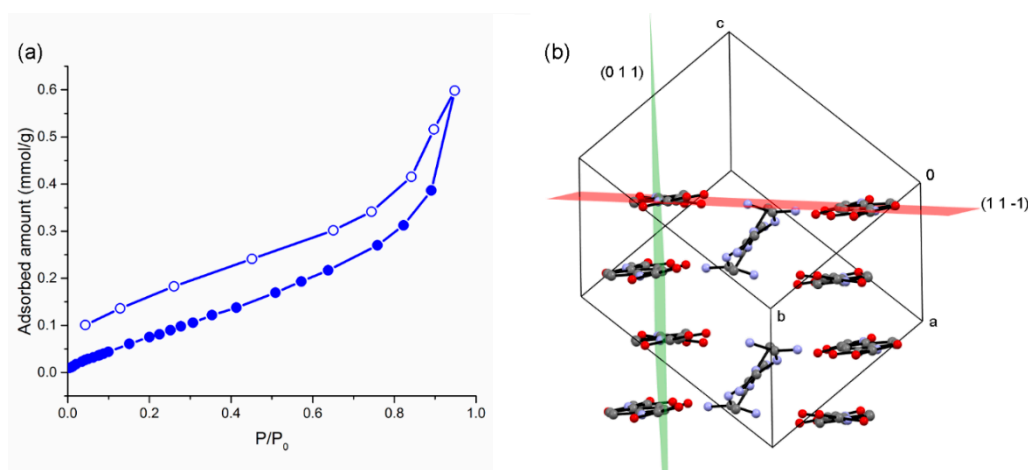


Figure 10. (a) Adsorption–desorption isotherm of $H_2Mf(HpOXA)_2$ under nitrogen, solid circles for adsorption and hollow circles for desorption. (b) View of the $H_2Mf(HpOXA)_2 \cdot 4W$ planes, water molecules are omitted. The hydrogen bonding network is weakened in the (1 1 -1) family of planes by the loss of four water molecules, but hydrogen bonding and $n \rightarrow \pi^*$ charge-assisted interactions prevail in the (0 1 1) family of planes.

3.4. The Nature and Structure of Dicationic Metformin in $H_2Mf(HpOXA)_2 \cdot 4W$ and $H_2Mf(HpOXA)_2$ Organic Salts

Metformin behaves as diprotic acid, whose pK_a values are referred to here as pK_{a1} and pK_{a2}, corresponding to H_2Mf^{2+}/HMf^+ and HMf^+/Mf acid–base conversions, respectively. The reported pK_a values are spread over a wide range depending upon the experimental method of measurement [36]. The pK_{a1} and pK_{a2} values are reported as being between 0.7–3.1 and 11.5–15.3 intervals, respectively. The formation of the organic salt $H_2Mf(HpOXA)_2 \cdot 4W$, vide supra, is explained by the proton transfer from H_2pOXA , as the acid, to HMf^+ , as the base. The ΔpK_a rule establishes that ionized acid–base molecular complexes, in the solid phase, are observed exclusively for $\Delta pK_a > 4$ [37]. The ΔpK_a is the difference between the pK_a of the base and the pK_a of the acid. Therefore, the ΔpK_a rule lead us to estimate the pK_{a1} value for the first deprotonation event of H_2pOXA in the -3.3 to -0.9 range, corresponding to a strong acid.

Furthermore, the protonation of the nitrogen bridge, in dicationic metformin, avoids the formation of the homodimer $R^2_2(8)$, raised by N–H...N interactions. This motif is frequently observed in the crystal structures of the monocationic metformin salts but absent in all dicationic known salts of metformin [6] including the tetrachlorocuprate [38]. Instead, a hydrogen bonding heterodimer $R^a_d(n)$ is formed in dicationic salts, with the participation of the anion group: $R^2_2(8)$ in the oxalic acid [30] and nitrate [39], $R^2_2(9)$ in squarate [40] and oxalamate monoacid (this work), $R^3_3(12)$ motif in sulfate [30] and $R^2_2(16)$ in sulfonatocalix [4,5]arenes [41]. The conformation in the form of an S backbone and the strongest acid on the nitrogen bridge seems to favor the hetero- over the homo-association. At this point, it is worth highlight the differences between metformin–carboxylate and metformin–oxalamate salts. The first forms the hydrogen bonding hetero-dimeric $R^2_2(8)$ motif, which has been found, in the crystal

network of guanidinium–carboxylate synthons [9]. This dominant motif is absent in the oxalamate salt $H_2Mf(HpOXA)_2 \cdot 4W$. Instead, the amide carbonyl of the $HpOXA^-$ moiety participates in the formation of the observed $R^2_2(9)$ motif and in the $n \rightarrow \pi^*$ charge-assisted interactions of mono- and bifacial type, herein described (see Table 2). Even when weak in strength, the $n \rightarrow \pi^*$ interaction, also named π -hole, has been found to be important for the stability of biomolecules and materials [42]. Because of the nature and bonding of the atoms involved, the carbonyl–guanidinium synthon $CO \cdots CN^+$ is similar to $CO \cdots CO$ interactions [32], but charge assisted. This synthon, as well as $H_2O \cdots CN^+$ synthon, is present, even when not described in the original sources, in the crystal network of metformin dicationic salts of squarate and oxalate. The analogous synthon $SO \cdots CN$ was identified in the crystal network of the acesulfame [43] and also in sulfonatocalix [4,5]arene metformin dicationic salts, in this last in the bifacial fashion $SO \cdots CN^+ \cdots OS$. Selected geometric parameters are listed in Table 6 to support the above discussion.

Table 6. Geometric parameters of regular $O(\delta^-) \cdots C(\delta^+)$ and bifacial $O(\delta^-) \cdots C(\delta^+) \cdots O(\delta^-)$ $n \rightarrow \pi^*$ interactions reported in H_2MfA organic salts (A = anion).

Organic Salt	X–O \cdots C	XO \cdots C/Å	X–O \cdots C/ $^\circ$	O \cdots C \cdots O/ $^\circ$	Me ₂ NCNC/ $^\circ$
$H_2Mf(HpOXA)_2 \cdot 4W$ (this work)	CO \cdots C54	3.142(3)	133.4(2)		148.8(2)
	CO \cdots C54	3.109(3)	131.8(2)	163.6(3)	
H_2Mf -squarate (1) ^a	CO \cdots C	3.212	148.0		–144.9
	H ₂ O \cdots C	3.156	167.5	136.3	
H_2Mf -squarate (2) ^a	CO \cdots C	2.988	87.9		143.3
	CO \cdots C	3.023	87.7		
H_2Mf -oxalate ^b	CO \cdots C	3.108	88.9		143.2
	H ₂ O \cdots C	3.152	158.3		
H_2Mf -sulfonatocalix[4,5]arenes ^c	SO \cdots C	2.938	132.2		41.4
	SO \cdots C	3.187	148.0	163.0	
H_2Mf -acesulfame ^d	SO \cdots C	3.130	128.1		141.6

^a [39], ^b [29] ^c [40], ^d [42].

It has been revealed that the $n \rightarrow \pi^*$ interaction can modulate the overall structural motifs even in the presence of strong hydrogen bonding interactions [44]. The results herein described for recurrent $n \rightarrow \pi^*$ charge-assisted interactions of mono- and bifacial type, in dicationic metformin salts, support the existence of these interactions independently, and not just as a short contact imposed by the geometric constraint due to the hydrogen bonding patterns. This $O(\delta^-) \cdots C(\delta^+)$ and $O(\delta^-) \cdots N^+$ could be responsible of the interactions of metformin in biologic systems.

4. Conclusions

The $H_2Mf(HpOXA)_2 \cdot 4W$ framework is given by ionic interactions of the H_2Mf^{2+} dication and two units of the $HpOXA^-$ monoanion. The inherent flexibility of both components is lost by the strong hydrogen bonding and $n \rightarrow \pi^*$ charge-assisted interactions between both moieties, whereas the main role of the water molecules is to equilibrate the number of hydrogen bonding acceptors in the crystal network. The vacant pockets left behind after water removal are preserved in the $H_2Mf(HpOXA)_2$ anhydrate, whose crystal network is stable and capable to rearrange in the presence of moisture to restore the microcrystalline lattice of the original tetrahydrate under proper conditions.

The formation of the organic salt $H_2Mf(HpOXA)_2 \cdot 4W$ implies the proton transfer from H_2pOXA , as the acid, to HMf^+ , as the base. The first deprotonation event of H_2pOXA was estimated in the –3.3 to –0.9 range, corresponding to a medium strength acid. The structure of metformin in the 1:2 salt $H_2Mf(HpOXA)_2 \cdot 4W$ is very similar to that observed in the monohydrates of the two other known dicationic 1:1 salts of formula $(H_2Mf)A \cdot H_2O$ (A = oxalate, sulfate). The conformation in the form of an S backbone and the strongest acid on the nitrogen bridge seems to favor the hetero-over the

homo-association; therefore, dicationic metformin is prone to hydrogen bonding with anions to form hetero $R^a_d(n)$ motifs. The *syn* conformation adopted by the N,N' -(1,4-phenylene)dioxalamic acid is uncommon among organic cocrystals, but is only attained by coordination to metals. The amide carbonyl of the HpOXA^- moiety participates in the formation of the observed $R^2_2(9)$ motif and in the $n \rightarrow \pi^*$ charge-assisted interactions of mono- and bifacial type. The $n \rightarrow \pi^*$ charge-assisted interactions should be taken into account in modelling the interaction of metformin with biological targets more than affecting the metformin therapeutic effects.

Author Contributions: Conceptualization, I.I.P.-M. and F.J.M.-M.; methodology, S.C.-C., A.A.R.-O.; formal analysis, S.C.-C. and E.V.G.-B.; writing—original draft preparation, S.C.-C., F.J.M.-M. and I.I.P.-M.; writing—review and editing and funding acquisition, I.I.P.-M. All authors have read and agreed to the published version of the manuscript.

Funding: This research was funded by CONACYT, grant number 255354 and Secretaría de Investigación y Posgrado del Instituto Politécnico Nacional, grant number 20170504.

Acknowledgments: This work was supported by CONACYT Grant 255354, SIP-IPN Grant 20170504 (Secretaría de Investigación y Posgrado del Instituto Politécnico Nacional), CONACYT “Red Temática de Química Supramolecular” Grant 271884. CGIC-UC (Coordinación General de Investigación Científica de la Universidad de Colima) and PROMEP-SEP. S.C.-C. thanks CONACYT for fellowship and I.I.P.-M. Thanks Susana Rojas-Lima of UAEH for the access to the X-ray diffractometer.

Conflicts of Interest: The authors declare no conflict of interest.

References

1. Shan, N.; Zaworotko, M.J. The role of cocrystals in pharmaceutical science. *Drug Discov. Today* **2008**, *13*, 441–446. [[CrossRef](#)]
2. Das, P.; Delost, M.D.; Qureshi, M.H.; Smith, D.T.; Njardarson, J.T. A Survey of the Structures of US FDA Approved Combination Drugs. *J. Med. Chem.* **2019**, *62*, 4265–4311. [[CrossRef](#)] [[PubMed](#)]
3. Bian, X.; Jiang, L.; Gan, Z.; Zhang, L.; Cai, L.; Hu, X. A Glimepiride-Metformin Multidrug Crystal: Synthesis, Crystal Structure Analysis, and Physicochemical Properties. *Molecules* **2019**, *24*, 3786. [[CrossRef](#)] [[PubMed](#)]
4. Bhatt, J.A.; Bahl, D.; Morris, K.; Stevens, L.L.; Haware, R.V. Structure-mechanics and improved tableting performance of the drug-drug cocrystal metformin-salicylic acid. *Eur. J. Pharm. Biopharm.* **2020**, *153*, 23–35. [[CrossRef](#)] [[PubMed](#)]
5. Plata-Vargas, E.; de la Cruz-Hernández, C.; Dorazco-González, A.; Fuentes-Noriega, I.; Morales-Morales, D.; Germán-Acacio, J.M. Synthesis of Metforminium Succinate by Melting. Crystal Structure, Thermal, Spectroscopic and Dissolution Properties. *J. Mex. Chem. Soc.* **2017**, *61*, 197–204. [[CrossRef](#)]
6. Kathuria, D.; Bankar, A.A.; Bharatam, P.V. What’s in a structure? The story of biguanides. *Mol. Struct.* **2018**, *1152*, 61–78. [[CrossRef](#)]
7. Hariharan, M.; Rajan, S.S.; Srinivasan, R. Structure of metformin hydrochloride. *Acta Cryst.* **1989**, *C45*, 911–913. [[CrossRef](#)]
8. Childs, S.L.; Chyall, L.J.; Dunlap, J.T.; Coates, D.A.; Stahly, B.C.; Stahly, G.P. A Metastable Polymorph of Metformin Hydrochloride: Isolation and Characterization Using Capillary Crystallization and Thermal Microscopy Techniques. *Cryst. Growth Des.* **2004**, *4*, 441–449. [[CrossRef](#)]
9. Nanubolu, J.B.; Sridhar, B.; Ravikumar, K.; Sawant, K.D.; Naik, T.A.; Patkar, L.N.; Cherukuvada, S.; Sreedhar, B. Polymorphism in metformin embonate salt-recurrence of dimeric and tetrameric guanidinium-carboxylate synthons. *Cryst. Eng. Commun.* **2013**, *15*, 4448–4464. [[CrossRef](#)]
10. González-González, J.S.; Martínez-Martínez, F.J.; García-Báez, E.V.; Cruz, A.; Morín-Sánchez, L.M.; Rojas-Lima, S.; Padilla-Martínez, I.I. Molecular Complexes of Diethyl N,N' -1,3-Phenyldioxalamate and Resorcinols: Conformational Switching through Intramolecular Three-Centered Hydrogen-Bonding. *Cryst. Growth Des.* **2014**, *14*, 628–642. [[CrossRef](#)]
11. Hall, C.M.; Wright, J.B. Antiallergic Phenylenedioxamic Acids. Ger. Offen DE 2362409 A1, 14 May 1980.
12. Wright, J.B.; Hall, C.M.; Johnson, H.G.J. N,N' -(phenylene)dioxamic acids and their esters as antiallergy agents. *Med. Chem.* **1978**, *21*, 930–935. [[CrossRef](#)] [[PubMed](#)]
13. Petyunin, G.P. Synthesis and pharmacological activity of phenylenedioxamic acids. *Khimiko-Farmatsevticheskii Zhurnal* **1986**, *20*, 827–830.

14. Oliveira, W.X.C.; Pinheiro, C.B.; da Costa, M.M.; Fontes, A.P.S.; Nunes, W.C.; Lloret, F.; Julve, M.; Pereira, C.L.M. Crystal Engineering Applied to Modulate the Structure and Magnetic Properties of Oxamate Complexes Containing the [Cu(bpca)]⁺ Cation. *Cryst. Growth Des.* **2016**, *16*, 4094–4107. [[CrossRef](#)]
15. Lisnard, L.; Chamoreau, L.-M.; Li, Y.; Journaux, Y. Solvothermal Synthesis of Oxamate-Based Helicate: Temperature Dependence of the Hydrogen Bond Structuring in the Solid. *Cryst. Growth Des.* **2012**, *12*, 4955–4962. [[CrossRef](#)]
16. Ramírez-Milanés, E.G.; Martínez-Martínez, F.J.; Magaña-Vergara, N.E.; Rojas Lima, S.; Avendaño-Jiménez, Y.A.; García-Báez, E.V.; Morín-Sánchez, L.M.; Padilla-Martínez, I.I. Positional isomerism and steric effects in the self-assemblies of phenylene bis-monothiooxalamides. *Cryst. Growth Des.* **2017**, *17*, 2513–2528. [[CrossRef](#)]
17. Gómez-Castro, C.Z.; Padilla-Martínez, I.I.; García-Báez, E.V.; Castrejón-Flores, J.L.; Peraza-Campos, A.L.; Martínez-Martínez, F.J. Solid state structure and solution thermodynamics of the three-centered hydrogen bond (O⋯H⋯O) using *N*-(2-benzoylphenyl) oxalyl derivatives as model compounds. *Molecules* **2014**, *19*, 14446–14460. [[CrossRef](#)] [[PubMed](#)]
18. Cabrera-Pérez, L.C.; García-Báez, E.V.; Franco-Hernández, M.O.; Martínez-Martínez, F.J.; Padilla-Martínez, I.I. Carbonyl–carbonyl interactions and amide π -stacking as the directing motifs of the supramolecular assembly of ethyl *N*-(2-acetylphenyl)-oxalamate in a synperiplanar conformation. *Acta Cryst.* **2015**, *C71*, 381–385.
19. Martin, S.; Beitia, J.I.; Ugalde, M.; Vitoria, P.; Cortes, R. Diethyl *N,N'*-*o*-phenylenedioxamate. *Acta Crystallogr. E Struct. Rep. Online* **2002**, *58*, o913–o915. [[CrossRef](#)]
20. James, S.L.; Adams, C.J.; Bolm, C.; Braga, D.; Collier, P.; Frišić, T.; Grepioni, F.; Harris, K.D.M.; Hyett, G.; Jones, W.; et al. Mechanochemistry: Opportunities for new and cleaner synthesis. *Chem. Soc. Rev.* **2012**, *41*, 413–447. [[CrossRef](#)]
21. Agilent. *CrysAlis PRO*; Agilent Technologies: Oxfordshire, UK, 2012.
22. Sheldrick, G.M. A short history of SHELX. *Acta Cryst.* **2008**, *A64*, 112–122. [[CrossRef](#)]
23. Farrugia, L.J. WinGX v2018.3 and ORTEP for windows: An update. *J. Appl. Cryst.* **2012**, *45*, 849–854. [[CrossRef](#)]
24. Sheldrick, G.M. Crystal structure refinement with SHELX. *Acta Cryst.* **2007**, *C71*, 3–8.
25. Spek, A.L. Single-crystal structure validation with the program PLATON. *J. Appl. Cryst.* **2003**, *36*, 7–13. [[CrossRef](#)]
26. Macrae, C.F.; Sovago, I.; Cottrell, S.J.; Galek, P.T.A.; McCabe, P.; Pidcock, V.; Platings, M.; Shields, G.P.; Stevens, J.S.; Towler, M.; et al. Mercury 4.0: From visualization to analysis, design and prediction. *J. Appl. Cryst.* **2020**, *53*, 226–235. [[CrossRef](#)] [[PubMed](#)]
27. Pardo, E.; Cangussu, D.; Lescouezec, R.; Journaux, Y.; Pasan, J.; Delgado, F.S.; Ruiz-Pérez, C.; Ruiz-García, R.; Cano, J.; Julve, M.; et al. Molecular-Programmed Self-Assembly of Homo- and Heterometallic Tetranuclear Coordination Compounds: Synthesis, Crystal Structures, and Magnetic Properties of Rack-Type CuII2MII2 Complexes (M = Cu and Ni) with Tetranucleating Phenylenedioxamato Bridging Ligands. *Inorg. Chem.* **2009**, *48*, 4661–4673. [[PubMed](#)]
28. Devi, R.N.; Jelsch, C.; Israel, S.; Aubert, E.; Anzline, C.; Hosamani, A.A. Charge density analysis of metformin chloride, a biguanide anti-hyperglycemic agent. *Acta Cryst.* **2017**, *B73*, 10–22.
29. Allen, F.H.; Kennard, O.; Watson, D.G.; Brammer, L.; Orpen, A.G.; Taylor, R. Tables of bond lengths determined by X-ray and neutron diffraction. Part 1. Bond lengths in organic compounds. *J. Chem. Soc. Perkin Trans. 2* **1987**, *12*, S1–S19. [[CrossRef](#)]
30. Lu, L.P.; Zhang, H.M.; Feng, S.S.; Zhu, M.L. Two *N,N*-dimethylbiguanidium salts displaying double hydrogen bonds to the counter-ions. *Acta Cryst.* **2004**, *C60*, o740–o743. [[CrossRef](#)]
31. Chernyshov, I.Y.; Ananyev, I.V.; Pidko, E.A. Revisiting van der Waals Radii: From Comprehensive Structural Analysis to Knowledge-Based Classification of Interatomic Contacts. *Chem. Phys. Chem.* **2020**, *21*, 370–376. [[CrossRef](#)]
32. Allen, F.H.; Baalham, C.A.; Lommerse, J.P.M.; Raithby, P.R. Carbonyl–Carbonyl Interactions can be Competitive with Hydrogen Bonds. *Acta Cryst.* **1998**, *B54*, 320–329. [[CrossRef](#)]
33. Kashid, S.M.; Sayan, B. Experimental Determination of the Electrostatic Nature of Carbonyl Hydrogen-Bonding Interactions Using IR–NMR Correlations. *J. Phys. Chem. Lett.* **2014**, *5*, 3211–3215. [[CrossRef](#)] [[PubMed](#)]
34. Suzuki, T.; Araki, T.; Kitaoka, H.; Terada, K. Characterization of Non-stoichiometric Hydration and the Dehydration Behavior of Sifafloxacin Hydrate. *Chem. Pharm. Bull.* **2012**, *60*, 45–55. [[CrossRef](#)] [[PubMed](#)]

35. Thommes, M.; Kaneko, K.; Neimark, A.V.; Olivier, J.P.; Rodriguez-Reinoso, F.; Rouquerol, J.; Sing, K.S.W. Physisorption of gases, with special reference to the evaluation of surface area and pore size distribution (IUPAC Technical Report). *Pure Appl. Chem.* **2015**, *87*, 1051–1069. [[CrossRef](#)]
36. Langmaier, J.; Pižl, M.; Samec, Z.; Zálíž, S. Extreme Basicity of Biguanide Drugs in Aqueous Solutions: Ion Transfer Voltammetry and DFT Calculations. *J. Phys. Chem. A* **2016**, *120*, 7344–7350. [[CrossRef](#)]
37. Cruz-Cabeza, A.J. Acid–base crystalline complexes and the pKa rule. *Cryst. Eng. Commun.* **2012**, *14*, 6362–6365. [[CrossRef](#)]
38. Lemoine, P.; Tomas, A. Tétrachlorocuprate(II) de metformine. *Acta Cryst.* **1994**, *C50*, 1437–1439. [[CrossRef](#)]
39. Fridrichová, M.; Císařová, I.; Němec, I. 1,1-Dimethylbiguanidium(2+) dinitrate. *Acta Cryst.* **2012**, *E68*, o18–o19. [[CrossRef](#)] [[PubMed](#)]
40. Šerb, M.D.; Kalf, I.; Englert, U. Biguanide and squaric acid as pH-dependent building blocks in crystal engineering. *Cryst. Eng. Commun.* **2014**, *16*, 10631–10639. [[CrossRef](#)]
41. Guo, D.S.; Zhang, H.Q.; Ding, F.; Liu, Y. Thermodynamic origins of selective binding affinity between *p*-sulfonatocalix[4,5]arenes with biguanidiniums. *Org. Biomol. Chem.* **2012**, *10*, 1527–1536. [[CrossRef](#)]
42. Bauzá, A.; Mooibroek, T.J.; Frontera, A. The Bright Future of Unconventional s/p-Hole Interactions. *Chem. Phys. Chem.* **2015**, *16*, 2496–2517. [[CrossRef](#)]
43. Wang, C.; Hu, S.; Sun, C.C. Expedited development of a high dose orally disintegrating metformin tablet enabled by sweet salt formation with acesulfame. *Int. J. Pharm.* **2017**, *532*, 435–443. [[CrossRef](#)] [[PubMed](#)]
44. Singh, S.K.; Das, A. The $n \rightarrow \pi^*$ interaction: A rapidly emerging non-covalent interaction. *Phys. Chem. Chem. Phys.* **2015**, *17*, 9596–9612. [[CrossRef](#)] [[PubMed](#)]

Publisher’s Note: MDPI stays neutral with regard to jurisdictional claims in published maps and institutional affiliations.



© 2020 by the authors. Licensee MDPI, Basel, Switzerland. This article is an open access article distributed under the terms and conditions of the Creative Commons Attribution (CC BY) license (<http://creativecommons.org/licenses/by/4.0/>).